Microstructural, Morphological, and Optical Study of Synthesis of ZnO and Pt-ZnO Nanoparticles by a Simple Method Using Different Precipitating Agents

Ruby S. Gines-Palestino, [a] Carlos Montalvo-Romero,[b] Guadalupe Luna-Solano,[a] Luis P. Amador-Gómez[a] and Denis Cantú-Lozano [*,a]

[a]*División de Estudios de Posgrado e Investigación, Instituto Tecnológico de Orizaba, CP 94320, Orizaba, Veracruz, Mexico*

[b]*Facultad de Química, Universidad Autónoma del Carmen, Ciudad del Carmen, CP 24180, Campeche, Mexico*

Due to its multiple applications, zinc oxide (ZnO) is one of the most used materials in science and technology. Therefore, this research carried out the synthesis of ZnO and Pt-ZnO nanoparticles (NPs) by the direct precipitation method, which is characterized by being simple and reproducible, using two different precipitating agents, potassium hydroxide (KOH) and sodium hydroxide (NaOH); for the doping of Pt-ZnO NPs was used platinum acetylacetone. To evaluate the effect of the precipitating agent on the properties of each doped material, they were characterized by Fourier transform infrared spectroscopy, where the Zn–O vibrations were more pronounced using KOH. X-ray diffraction analysis shows a hexagonal structure (wurtzite) formation for ZnO with NaOH, obtaining a smaller crystal size than the other synthesized materials. Scanning electron microscopy analysis showed hexagonal and hemispherical shapes for ZnO (with NaOH and KOH) and Pt-ZnO (with NaOH), respectively; also, cylindrical shapes were obtained for Pt-ZnO (with KOH). The highest band gap obtained was for the Pt-ZnO material synthesized with KOH.

Keywords: nanoparticles, synthesis, precipitation, zinc oxide, platinum

Introduction

Zinc oxide (ZnO) is a compound that has attracted the attention of the scientific community because many industries rely on it to develop new materials. ZnO is a white chemical compound belonging to family II-VI, with a band gap of 3.37 eV.[1] It is considered one of the most ionic compounds of this family due to the difference in electronegativities that exist in zinc and oxygen, forming a high degree of ionicity in its bond.[2] It can have three crystal structures: wurtzite, zinc mixture, and rock salt. The wurtzite-type phase is the most stable under normal pressure and temperature conditions; the zinc blend phase can only be stabilized by growth on cubic substrates, and the rock salt phase is obtained at high pressures.[3]

ZnO has a wide variety of commercial applications, such as in the rubber, ceramic, paint, chemical reagents, and agricultural industries, at low cost.[4,5] It can be applied in science and technology as catalysts since they have great potential in photocatalysis applications,[6] due to their excellent properties: optical, high infrared reflectivity, acoustic characteristics, chemical stability, high electrochemical sensitivity, and excellent electronic properties, being considered as a multifunctional material.[7,8]

Heterogeneous photocatalysis to degrade pollutants uses a semiconductor material that produces an accelerated reaction using light irradiation; the catalyst accelerates the reaction rate by reducing the activation energy; this process depends on the ability of the photocatalyst to collect light and create electron-hole pairs.[9] The formation of electrons and holes is responsible for forming active sites on the semiconductor surface, which favors the formation of free radicals capable of degrading several dyes from aqueous solutions and many other environmental pollutants, being more efficient than other catalysts such as TiO_2.[10]

The photocatalytic performance of ZnO is closely related by its morphology, particle size, crystallinity, crystalline orientation, and optical properties.[11] Research in the synthesis of nanomaterials is directed to control their shape, size, and composition; these characteristics are of utmost importance to determining the properties of the

materials that lead to different technological applications,[7] among them the application of photocatalytic materials. Various techniques can synthesize ZnO nanoparticles (NPs),[12] such as hydrothermal,[13] microemulsions,[14] solvothermal,[15] photo deposition,[16] sol-gel,[17] pyrolyzes,[18] and precipitation method[7] that is one of the most cost-effective and simple methods; it requires simple equipment for producing homogeneous materials using various parameters such as temperature control and precursor concentration.[9]

The practical application of semiconductor ZnO as a catalyst is mainly hampered by its band gap and rapid recombination of photo-induced charge carriers. Therefore, ZnO should be modified by structural doping with both metallic and non-metallic materials to increase its photocatalytic potential and the sensitivity of ZnO toward visible and ultraviolet light.[19] Doping the semiconductor with a nanoscopic metal or metal oxide provides a low recombination rate of electron-hole pairs, increasing photocatalytic activity of ZnO.[20]

Currently, most studies focus on doping ZnO with other metals; however, there are few investigations on doping Pt nanoparticles on ZnO. This research synthesized ZnO and Pt-ZnO NPs by modifying the precipitation method, which is considered one of the most reliable, easy, and reproducible, using two precipitating agents: KOH and NaOH. In order to evaluate the influence of the precipitating agent on the yield, composition, and morphology, the nanomaterials were characterized using different techniques: Fourier transform infrared spectroscopy (FTIR) to determine the structural and molecular properties of the obtained materials,[21] X-ray diffraction (XDR) which was used to calculate structural parameters,[22] scanning electron microscopy (SEM) which was used to determine the morphology and size of the nanoparticles,[19] and finally optical analysis by UV-Vis spectroscopy,[23] to calculate the band gap of the synthesized materials in order to evaluate which material is the most suitable for use as a photocatalyst in the degradation of recalcitrant compounds; it is estimated that in sectors of recovery of water, air, and soil are contaminated with recalcitrant compounds valued at 1,000,000 million dollars.[24]

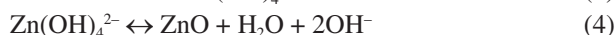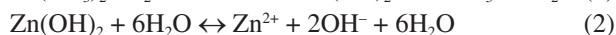## Experimental

Chemical products and reagents

The reagents used for the synthesis of the catalysts were zinc nitrate hexahydrate ($Zn(NO_3)_2 \cdot 6H_2O$, ≥ 99%, Meyer, Mexico), potassium hydroxide (KOH, ≥ 85%, Meyer,

Mexico), sodium hydroxide (NaOH, ≥ 98.4%, Fermont, Mexico), platinum acetylacetonate ($C_{10}H_{14}O_4Pt$, ≥ 97%, Sigma-Aldrich, Mexico), acetone (($CH_3)_2CO$, ≥ 99.6%, JT Baker, Mexico), ethanol (C_2H_6O, ≥ 99%, Jalmek, Mexico), and distilled water (Wöhler, Mexico).
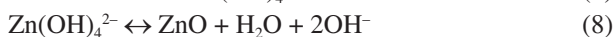
Synthesis of ZnO and Pt-ZnO

The synthesis of the ZnO semiconductor was performed using the modification of the direct precipitation technique.[11] The first semiconductor was performed with a solution of 0.2 M Zn $(NO_3)_2 \cdot 6H_2O$, which was added to a solution of 0.4 M KOH under magnetic stirring (with a flow rate of 6 mL *per* min) as first precipitating agent. For the second semiconductor, a solution of 0.2 M Zn $(NO_3)_2 \cdot 6H_2O$ was added by magnetic stirring (with a flow rate of 6 mL min^{-1}), and a 1 M NaOH solution as a second precipitating agent was used. The precipitates were filtered and washed with distilled water and ethanol, dried in an oven (Felisa, Mexico) (100 ºC, 24 h), and then calcined in a muffle (Felisa, Mexico) (500 ºC, 3 h).

The reaction mechanism for the precursor zinc nitrate hexahydrate ($Zn(NO_3)_2 \cdot 6H_2O$) with the precipitating agent potassium hydroxide (KOH) is as follows: at the onset of the reaction, Zn^{2+} and OH^- ions coordinate with each other to dehydrate by proton transfer forming $Zn^{2+}...O^{2-}......Zn^{2+}$ bonds, giving rise to an agglomerate of the form of $[Zn_x(OH)_y]^{(2x-y)+}$, that has an octahedral structure. Initially, these aggregates usually contain less than 50 ions, and forming O^{2-} involves dramatic changes within the agglomerate. H_2O molecules formed by dehydration migrate into the solution as the process progresses. When the aggregates reach 150 ions, the wurtzite structure is built, which has tetrahedral coordination. The core consists of Zn^{2+} and O^{2-} ions, while the surface remains the Zn^{2+} and OH^- ions aggregate. The aggregates larger than 200 ions show a core in nanometer size which will grow because of the same process that gave formation to them, i.e., through the association of Zn^{2+} and OH^- ions, the loss of hydrogen from it, and incorporation into the already formed crystals.[3,14] The reactions of the synthesis process for the KOH precipitant are shown in the following equations 1-4:

$$Zn(NO_3)_2 \cdot 6H_2O + 2KOH \leftrightarrow Zn(OH)_2 + 2KNO_3 + 6H_2O \quad (1)$$
$$Zn(OH)_2 + 6H_2O \leftrightarrow Zn^{2+} + 2OH^- + 6H_2O \quad (2)$$
$$Zn^{2+} + 2OH^- \leftrightarrow Zn(OH)_4^{2-} \quad (3)$$
$$Zn(OH)_4^{2-} \leftrightarrow ZnO + H_2O + 2OH^- \quad (4)$$

The second synthesis of ZnO (equations 5-8) shows the reaction mechanism for zinc nitrate hexahydrate

$(Zn(NO_3)_2 \cdot 6H_2O)$ with the precipitating agent sodium hydroxide (NaOH) by the precipitation synthesis method.[25,26]

$$Zn(NO_3)_2 \cdot 6H_2O + 2NaOH \leftrightarrow Zn(OH)_2 + 2NaNO_3 + 6H_2O \quad (5)$$
$$Zn(OH)_2 + 6H_2O \leftrightarrow Zn^{2+} + 2OH^- + 6H_2O \quad (6)$$
$$Zn^{2+} + 2OH^- \leftrightarrow ZN(OH)_4^{2-} \quad (7)$$
$$Zn(OH)_4^{2-} \leftrightarrow ZnO + H_2O + 2OH^- \quad (8)$$

Using the incipient impregnation technique,[27] the platinum nanoparticles (Pt-ZnO) were doped in the two semiconductors based on different precipitating agents. A 0.5% platinum acetylacetonate solution diluted in acetone was prepared, drip-added to each semiconductor over a heating grid at 90 °C, and catalyzers were calcined at 400 °C for two hours.

Fourier-transformed infrared spectroscopy (FTIR) characterization

Fourier transform infrared spectroscopy (FTIR) was performed with a spectrometer (Agilent Cary, Malaysia) with a scanning range of 4000 to 400 cm^{-1} with attenuated total reflectance (ATR).

Structural analysis by X-ray diffraction (XRD)

The equipment used to evaluate the crystalline nature of synthesized materials was a diffractometer (Rigaku Ultima, Japan) with a thin film module (Cu radiation Kα $\lambda = 0.15418$ nm, 40 kV, 44 mA and angle step of 0.02°) in the Bragg-Brentano configuration. Subsequently, the results obtained were analyzed with Match! 3.0[28] software to compare it with the ZnO pattern. The crystal size was determined using by Scherrer formula using equation 9.[22]

$$\text{Crystal size (D)} = \frac{K\lambda}{\beta \cos\theta} \quad (9)$$

where D (nm) is the average diameter of the crystal, λ (nm) is the wavelength of X-ray radiation Cu Kα ($\lambda = 0.15418$ nm), K is the shape factor, β is full-width half maximum intensity (FWHM), and θ is the Bragg's angle.[15]

Different factors determine the crystal characteristics, such as peak broadening, dislocation density (δ), lattice constants (a and c), interplanar distance (d), unit cell volume (V), density (ρ), number of unit cells in a particle (n) and strain (ε); these factors were determined by equations 10-16.[23]

$$\text{Dislocation density } (\delta) = \frac{1}{D^2} \quad (10)$$

$$\text{Inter-planner spacing } \frac{1}{d^2_{(hkl)}} = \left(\frac{h^2 + k^2}{a^2}\right) + \frac{t^2}{c^2} \quad (11)$$

$$\text{Volume (V)} = a^2 c \quad (12)$$

$$\text{Density } (\rho) = \frac{nM}{NV} \quad (13)$$

$$\text{Number of unit cells in a particle (n)} = \frac{4}{3\pi\left(\dfrac{D}{2v}\right)} \quad (14)$$

$$\text{stress} (\varepsilon) = \frac{\beta_{hkl}}{4 \tan\theta} \quad (15)$$

$$\text{Specific surface area (SSA)} = \frac{6000}{Dp} \quad (16)$$

where SSA (m^2 g^{-1}) is the specific surface area, M (g mol^{-1}) is molecular weight, V (Å^3) is unit cell volume, N (mol^{-1}) is Avogadro's number, and ρ (g cm^{-3}) is the density of the catalyst.[23]

Morphology study by scanning electron microscopy (SEM)

To know the morphology of the synthesized ZnO and Pt-ZnO nanocatalysts, scanning electron microscopy (SEM) analysis was performed with INSTRUMENT JSM-6490 equipment (North Billerica, Massachusetts, USA), with a voltage of 20 kV and a magnification of 10 000×, the micrographs were interpreted in ImageJ[29] software to determine the approximate diameter of the nanoparticles.

Optical analysis by UV-Vis spectroscopy

For the determination of the band gap, it was necessary to perform an optical analysis; 50 mg of each of the catalysts were diluted in 100 mL of distilled water for 10 min of constant stirring; the dilutions of each of the catalysts were measured in absorbance mode, with a resolution of 0.05 nm with scans in the wavelength range between 200 and 500 nm using a GENESYS 10S Thermo Scientific ultraviolet-visible (UV-Vis) spectrophotometer (UV-Vis).[30-32]

The bandgap energy of these synthesized nanomaterials (ZnO and Pt-ZnO) was determined using the Kubelka-Munk (equation 17) by the Tauc Plot method by plotting $(\alpha h\upsilon)^n$ *versus* $h\upsilon$ and extrapolating the linear parts of the curves.[30-35]

$$(\alpha h\upsilon) = A(h\upsilon - E_g)^n \quad (17)$$

where E_g is the band gap of the semiconductor (eV), h is the Planck constant (J s), υ is the frequency of light (s^{-1}), A is the absorption constant, *n* is an index with different

J. Braz. Chem. Soc. **2024**, *35*, 1, e-20230092

3 of 13

values (1/2 for direct allowed, 2 for indirect allowed, 3/2 for direct forbidden, and 3 for indirect forbidden), and α is the absorption coefficient (defined by the Beer-Lambert law) as equation 18.[36]

$$\alpha = ([2{,}303 \times Abs]/d) \qquad (18)$$

where *d* is the thickness of the sample, and Abs is absorbance.

Results and Discussion

Fourier-transformed infrared spectroscopy (FTIR) characterization

Figure 1 shows the overlaid spectra of ZnO and Pt-ZnO using two different precipitating agents: KOH and NaOH. Bands are observed between 3500-3200 cm⁻¹ belonging to the O–H groups coordinated with zinc ions due to the presence of water on the surface of the nanoparticles.[37] The bands 2927-2854 cm⁻¹ correspond to alkanes.[25]
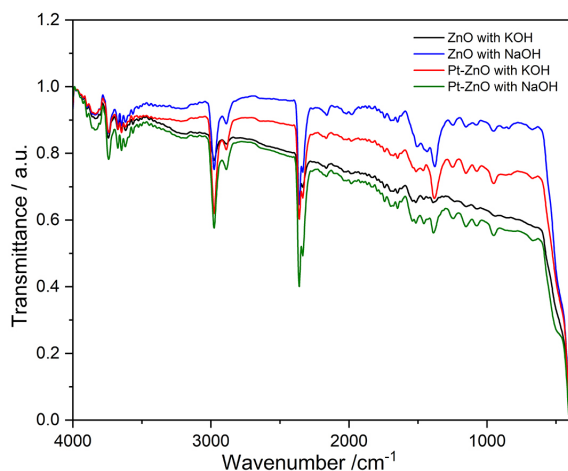

Figure 1. FTIR-ATR of ZnO and Pt-ZnO NPs with KOH and NaOH precipitating agents.

The spectra of ZnO with KOH present the absorption band at 1385 cm⁻¹ corresponding to the bonding between potassium and oxygen; these bonds were due to the thermal decomposition of KOH at 500 °C producing oxide.[38] In the spectra of ZnO with NaOH, weak bands at 1384 cm⁻¹ were observed due to vibrations of Zn–O bonds, and the bands at 1050-700 cm⁻¹ were also due to Zn–O bonds.[37]

The absorption at 874 cm⁻¹ was due to the formation of tetrahedral coordination of Zn. The weak bands observed from 660 to 400 cm⁻¹ were due to vibrations of Zn–O NPs. The peak at 604 cm⁻¹ indicates the stretching of the Zn–O bond,[27] being the most pronounced band of the ZnO synthesized with NaOH.

In the spectra of Pt-doped catalysts, prominent bands can be observed at 1200-1000 cm⁻¹; the intensity of the 1200 cm⁻¹ peak increased with the addition of Pt in ZnO.[39]

X-ray diffraction (XDR)

All the catalysts derived from different precursors (KOH and NaOH) were analyzed using XRD. The ZnO and Pt pattern according to the Crystallography Open Database (COD) and ZnO and Pt-ZnO NPs derived from different precursors (KOH and NaOH) are shown in Figure 2.

In Figure 2a (ZnO NPs with KOH), the highest peaks were found at 31.75° (1 0 0), 34.41° (0 0 2), 36.23° (1 0 1), 47.51° (0 1 2), 56.57° (1 1 0), 62.81° (0 1 3), 66.35° (2 0 0), 67.91° (1 1 2), 69.05° (2 0 1), 72. 55° (0 0 4), 76.91° (2 0 2), which clearly show the hexagonal crystal structure of ZnO. The value of the maximum peaks coincides with the COD-2300450 standard, and no other diffraction peaks were detected. The smallest crystal was in the (2 0 2) plane, and the average crystal size was 53.17 nm.

The characterization results for ZnO NPs with NaOH are observed in Figure 2b. The highest peaks were found at 31.8° (1 0 0), 34.46° (0 0 2), 36.28° (1 0 1), 47.6° (0 1 2), 56.66° (1 1 1), 62.92° (0 1 3), 66.44° (2 0 0), 68.02° (1 1 2), 69.14° (2 0 1), 72.66° (0 0 4), 77.04° (2 0 2) which coincide with the COD-2300450 standard presented a hexagonal crystal structure. The smallest crystal size was found in the (0 1 3) plane due to low-intensity peak, dislocation density, and strain.

Pt-ZnO NPs were analyzed with KOH precipitating agent; we can observe in Figure 2c that the highest peaks are found at 31.76° (1 0 0), 34.42° (0 0 2), 36.25° (1 0 1), 47.53° (0 1 2), 56.58° (1 1 1 0), 56.93° (1 0 −1), 62.84° (0 1 3), 66.35° (2 0 0), 67. 92° (1 1 2), 69.06° (2 0 1), 72.54° (0 0 4), 76.93° (2 0 2), platinum was observed at peak (1 0 −1) according to COD-1001824 standard. The smallest crystal size was found at the (1 0 0) plane due to a high-intensity peak and smaller displacement; the largest crystal size was found at the (2 0 2) plane due to its width and lower dislocation density compared to the other planes.

The results of doping the Pt-ZnO NPs with the precipitating agent NaOH were observed in Figure 2d. The highest peaks were found at 31.8° (1 0 0), 34.46° (0 0 2), 36.28° (1 0 1), 47.6° (0 1 2), 56.66° (1 1 1), 62.92° (0 1 3), 66.39° (0 2 0), 66. 45° (2 0 0), 68.02° (1 1 2), 69.14° (2 0 1), 72.66° (0 0 4), 77.04° (2 0 2), platinum was detected at peak (0 2 0) according to COD-1001825 standard. The smallest crystal size was found at the (1 0 0) plane due to a high-intensity peak and smaller displacement; the largest was found at the (0 1 3).
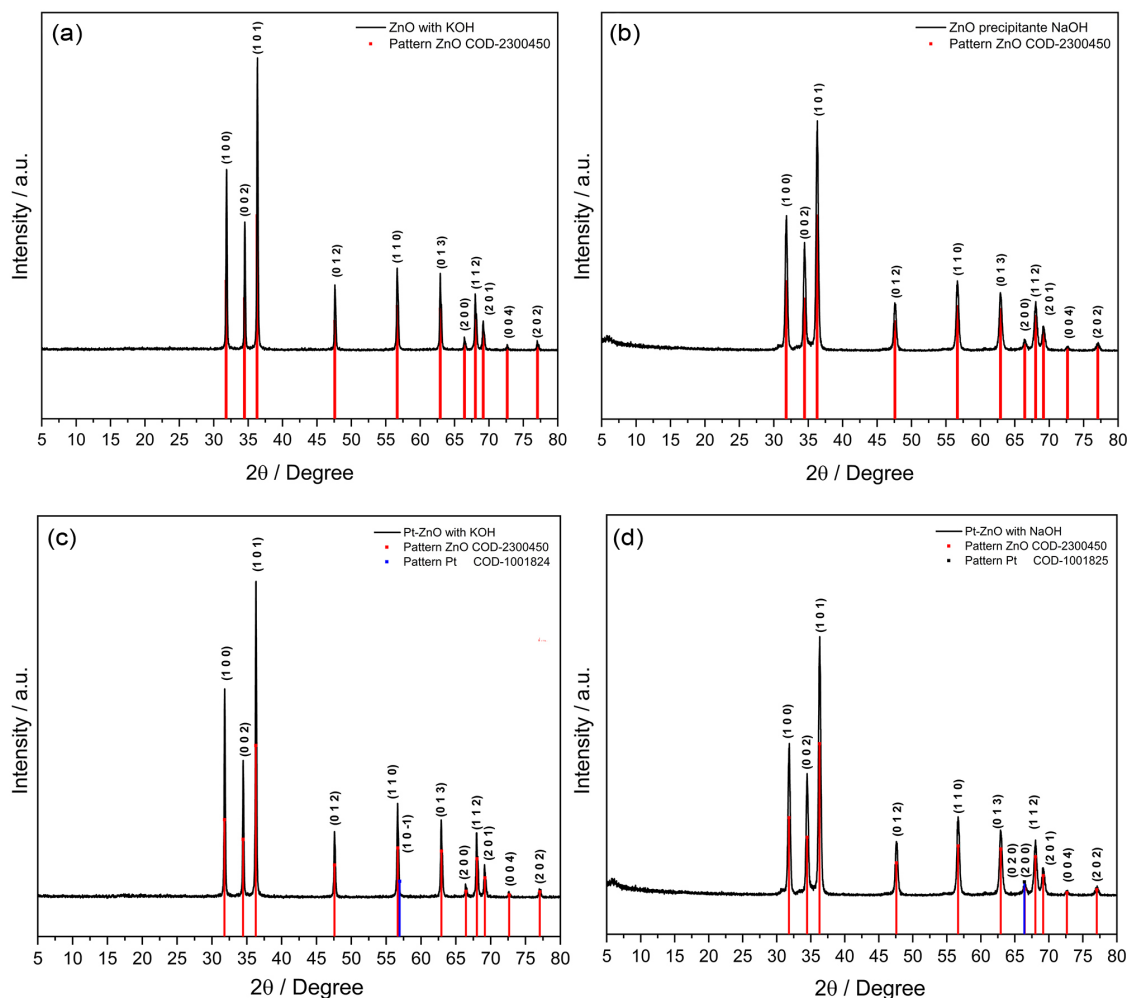
Figure 2. XRD of catalyst synthesis (a) ZnO with KOH precipitating agent, (b) ZnO with NaOH, (c) Pt-ZnO with KOH, and (d) Pt-ZnO with NaOH.

The results of the crystallographic parameters for each synthesized material are shown in Table 1. It can be observed that the irregularities of the crystal structure were directly related to the dislocation density. When the dislocation density decreases, the deformation also decreases, which causes the crystal size to increase.

The average crystal size obtained for ZnO NPs with NaOH was 23.63 nm, with a deviation of ± 4.48. The average crystal size obtained for ZnO NPs with KOH was ± 53.17 nm, with a deviation of ± 15.99. The crystal size results with NaOH precipitating agent are smaller than those obtained with KOH precipitating agent; the smaller crystal size increases the photocatalytic power, so ZnO with NaOH precipitating agent could have better results by having a smaller crystal size.

The average crystal size obtained for Pt-ZnO NPs with KOH was 57.21 nm with a deviation of ± 3.96; an increase in crystal size is observed compared to undoped ZnO due to the addition of the metal compound.

The average crystal size obtained for Pt-ZnO NPs with NaOH was 24.14 nm with a deviation of ± 4.61; comparing the crystal size of the two platinum-doped semiconductors, we can observe that the desired size was obtained by synthesizing the semiconductor with NaOH since the catalyst has a smaller size than a semiconductor with KOH; a smaller crystal size favors the photocatalytic potential of the catalyst.

With the data obtained from the diffractograms, we could calculate several factors, which allowed us to have a broader knowledge of the crystal structure (Table 2); it is observed that the density of the doped materials increases with the addition of platinum. The average crystal size shows that the smaller the deformation, the larger the crystal size.

Figures 3 and 4 show the relationship between crystal size with dislocation density and deformation of materials synthesized with different precipitating agents: NaOH and KOH.

The results show that crystallite size depends on dislocation density and deformation. The displacement or

J. Braz. Chem. Soc. **2024**, *35*, 1, e-20230092

5 of 13

Table 1. Crystallographic parameters of XRD characterization for ZnO with KOH, ZnO with NaOH, Pt-ZnO with KOH, and Pt-ZnO with NaOH

ZnO with KOH	2θ / degree	(hkl)	FWHM β / degree	FWHM β / rad	Crystallite size (D) / nm	Dislocation density (δ)	Strain (ε)
	31.75	(1 0 0)	0.2	0.00349	41.32863	0.00059	0.00307
	34.41	(0 0 2)	0.2	0.00349	41.61453	0.00058	0.00282
	36.23	(1 0 1)	0.2	0.00349	41.82549	0.00057	0.00267
	47.51	(0 1 2)	0.16	0.00279	54.29014	0.00034	0.00159
	56.57	(1 1 0)	0.2	0.00349	45.14231	0.00049	0.00162
	62.81	(0 1 3)	0.16	0.00279	58.21930	0.00030	0.00114
	66.35	(2 0 0)	0.24	0.00419	39.57809	0.00064	0.00160
	67.91	(1 1 2)	0.2	0.00349	47.92467	0.00044	0.00130
	69.05	(2 0 1)	0.2	0.00349	48.25027	0.00043	0.00127
	72.55	(0 0 4)	0.12	0.00209	82.18194	0.00015	0.00071
	76.91	(2 0 2)	0.12	0.00209	84.60509	0.00014	0.00066
ZnO with NaOH							
	31.8	(1 0 0)	0.36	0.00628	22.96320	0.00190	0.00551
	34.46	(0 0 2)	0.32	0.00559	26.01260	0.00148	0.00450
	36.28	(1 0 1)	0.36	0.00628	23.23970	0.00185	0.00479
	47.6	(0 1 2)	0.4	0.00698	21.72357	0.00212	0.00396
	56.66	(1 1 0)	0.4	0.00698	22.58071	0.00196	0.00324
	62.92	(0 1 3)	0.48	0.00838	19.41782	0.00265	0.00342
	66.44	(2 0 0)	0.44	0.00768	21.59915	0.00214	0.00293
	68.02	(1 1 2)	0.44	0.00768	21.79804	0.00210	0.00285
	69.14	(2 0 1)	0.44	0.00768	21.94380	0.00208	0.00279
	72.66	(0 0 4)	0.44	0.00768	22.42907	0.00199	0.00261
Pt-ZnO with KOH							
	31.76	(1 0 0)	0.1599	0.00279	51.69438	0.00037	0.00245
	34.42	(0 0 2)	0.1599	0.00279	52.05210	0.00037	0.00225
	36.25	(1 0 1)	0.1599	0.00279	52.31755	0.00037	0.00213
	47.53	(0 1 2)	0.1599	0.00279	54.32827	0.00034	0.00158
	56.58	(1 1 0)	0.1599	0.00279	56.46583	0.00031	0.00130
	56.93	(1 0 -1)	0.1599	0.00279	56.55907	0.00031	0.00129
	62.84	(0 1 3)	0.1599	0.00279	58.26502	0.00029	0.00114
	66.35	(2 0 0)	0.1599	0.00279	59.40426	0.00028	0.00107
	67.92	(1 1 2)	0.1599	0.00279	59.94682	0.00028	0.00104
	69.06	(2 0 1)	0.1599	0.00279	60.35418	0.00027	0.00101
	72.54	(0 0 4)	0.1599	0.00279	61.67105	0.00026	0.00095
	76.93	(2 0 2)	0.1599	0.00279	63.50230	0.00025	0.00088
Pt-ZnO with NaOH							
	31.8	(1 0 0)	0.36	0.00628	22.96320	0.00190	0.00551
	34.46	(0 0 2)	0.32	0.00559	26.01260	0.00148	0.00450
	36.28	(1 0 1)	0.36	0.00628	23.23970	0.00185	0.00479
	47.6	(0 1 2)	0.4	0.00698	21.72357	0.00212	0.00396
	56.66	(1 1 0)	0.4	0.00698	22.58071	0.00196	0.00324
	62.92	(0 1 3)	0.48	0.00838	19.41782	0.00265	0.00342
	66.39	(0 2 0)	0.3198	0.00558	29.70891	0.00113	0.00213
	66.44	(2 0 0)	0.44	0.00768	21.59915	0.00214	0.00293
	68.02	(1 1 2)	0.44	0.00768	21.79804	0.00210	0.00285
	69.14	(2 0 1)	0.44	0.00768	21.94380	0.00208	0.00279
	72.66	(0 0 4)	0.44	0.00768	22.42907	0.00199	0.00261

FWHM β: full-width half maximum intensity.

Table 2. The calculated average of structural parameters of the different synthesized materials

Parameter	Calculated values			
Catalyst	ZnO with NaOH	ZnO with KOH	Pt-ZnO with NaOH	Pt- ZnO with KOH
Average crystallite size (D) / nm	23.63 ± 4.48	53.17 ± 15.99	24.14 ± 4.61	57.21 ± 3.96
Average dislocation density (δ)	0.00191	0.00042	0.00185	0.00030
Cell constant / Å	a = 3.2494 c = 5.2024	a = 3.2494 c = 5.2024	a = 3.2494 c = 5.2024	a = 3.2494 c = 5.2024
Density (ρ) / (g cm^{-3})	4.920	4.920	16.715	16.715
Specific surface area (SSA) / (m^2 g^{-1})	51.60	22.93	14.86	6.27
Strain (ε)	0.00346	0.00168	0.00336	0.00142

broadening of the peaks is directly related to the deformation of the materials. Peak shift refers to homogenous strain, and peak broadening to inhomogeneous strain, which reduces the size of the crystallites.

The dislocation density was due to irregularity or cracks in the crystal structure. The increase in dislocation density increases strain, which decreases the crystallite size.

Figures 4c, 4d, 4g, and 4h show the deformation-induced peak broadening in the crystallite size. The results obtained show that the crystal size reduces as the deformation increases.

The broadening stops increasing when strain reaches a certain limit, known as inherent instrumental broadening. Figure 4 shows the strain-induced instrumental peak broadening effect on crystallite size. The result infers that the crystallite size decreases as strain increases, beyond which the crystallite size tends to increase. This confirms that the crystallite size could be larger for higher strain present in the crystallite structure.
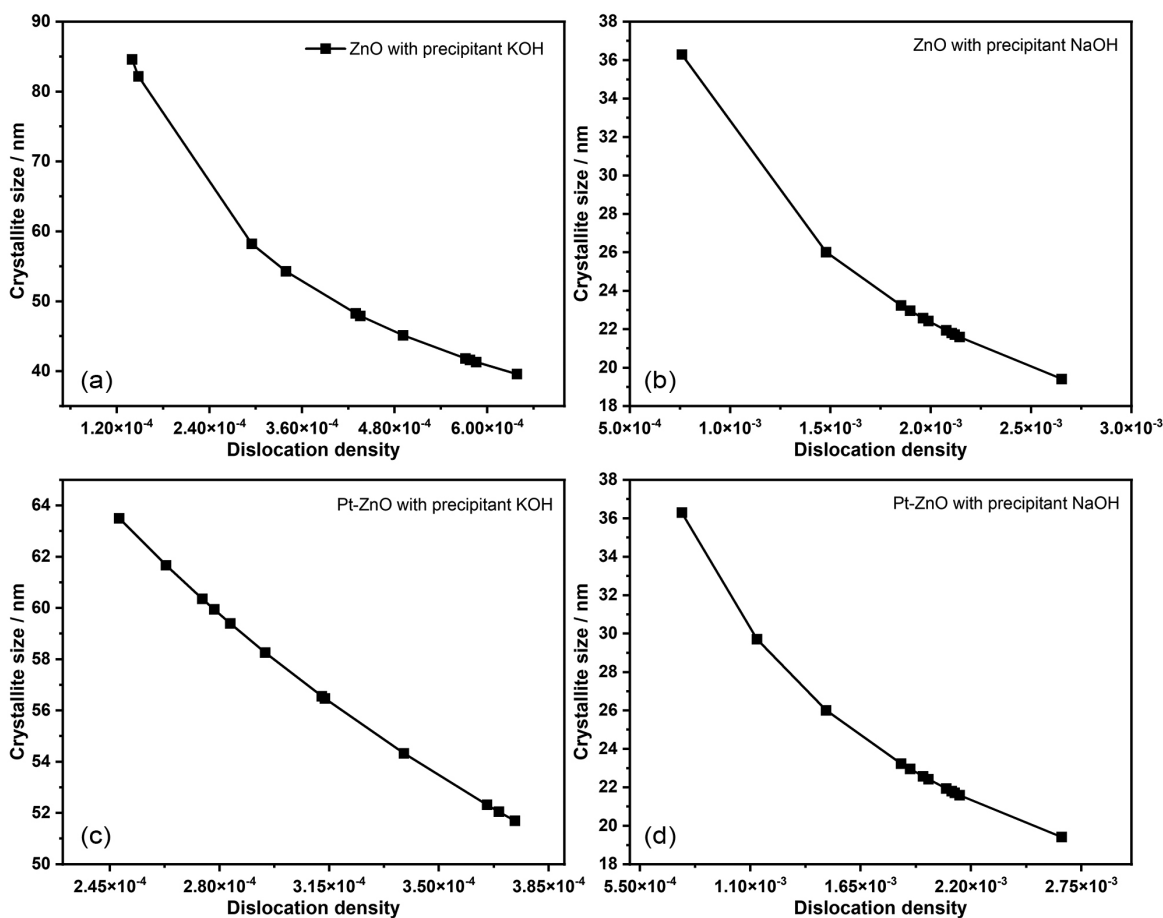

Figure 3. Variation of crystal size with a dislocation density of synthesized materials, (a) ZnO with KOH, (b) ZnO with NaOH, (c) Pt-ZnO with KOH, (d) Pt-ZnO with NaOH.
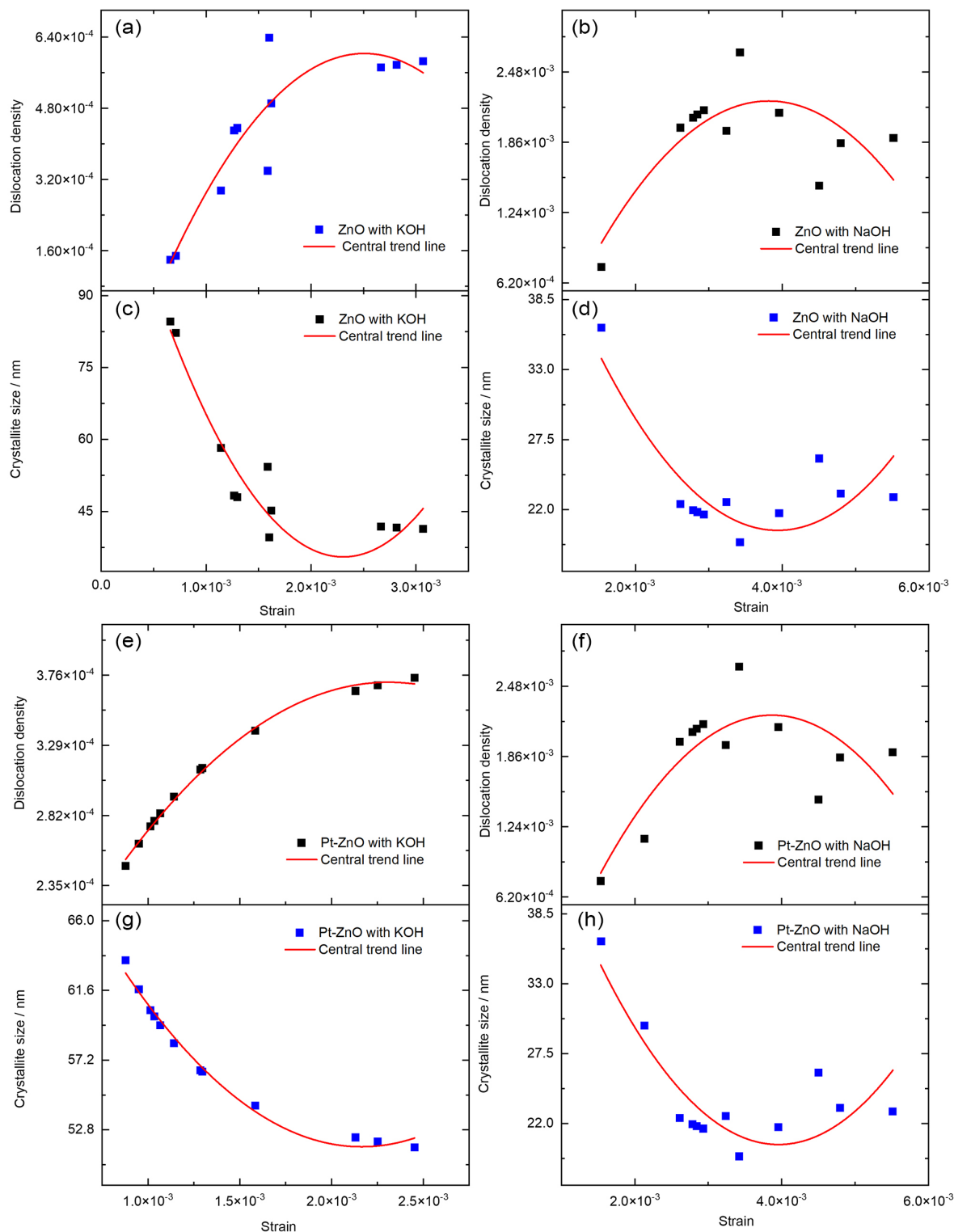
Figure 4. Deformation *vs.* dislocation density and stress *vs.* crystalline size of the different synthesized materials.

Morphology study by scanning electron microscopy (SEM)

ZnO can adopt different structures depending on the type of precursor used.[40] The most common structures discovered correspond to nanotubes, nanorods, nanobelts, nanowires, and nanorings, among others.[41,42]

The various morphologies of ZnO depend significantly on NaOH and KOH.[1] The morphology and particle size distribution of ZnO and Pt-ZnO are shown in Figure 5, where the particles' polyhedral grains and crystalline

structure can be observed, confirming the nano dimensions and the high degree of crystallinity of the synthesized particles.[43]

The ZnO and Pt-ZnO NPs have a hexagonal shape homogeneously distributed with some agglomerated particles with an average diameter of about 114.10 nm at precipitating agent KOH (Figure 5a); a hexagonal shape

of about 92.64 nm and agglomerates in different directions with precipitating agent NaOH (Figure 5b); rod-like structure with homogeneous distribution and mean diameter of about 99.70 nm at KOH (Figure 5c); and semi-spherical shape an average diameter of about 102.39 nm with a non-homogeneous distribution at NaOH (Figure 5d).

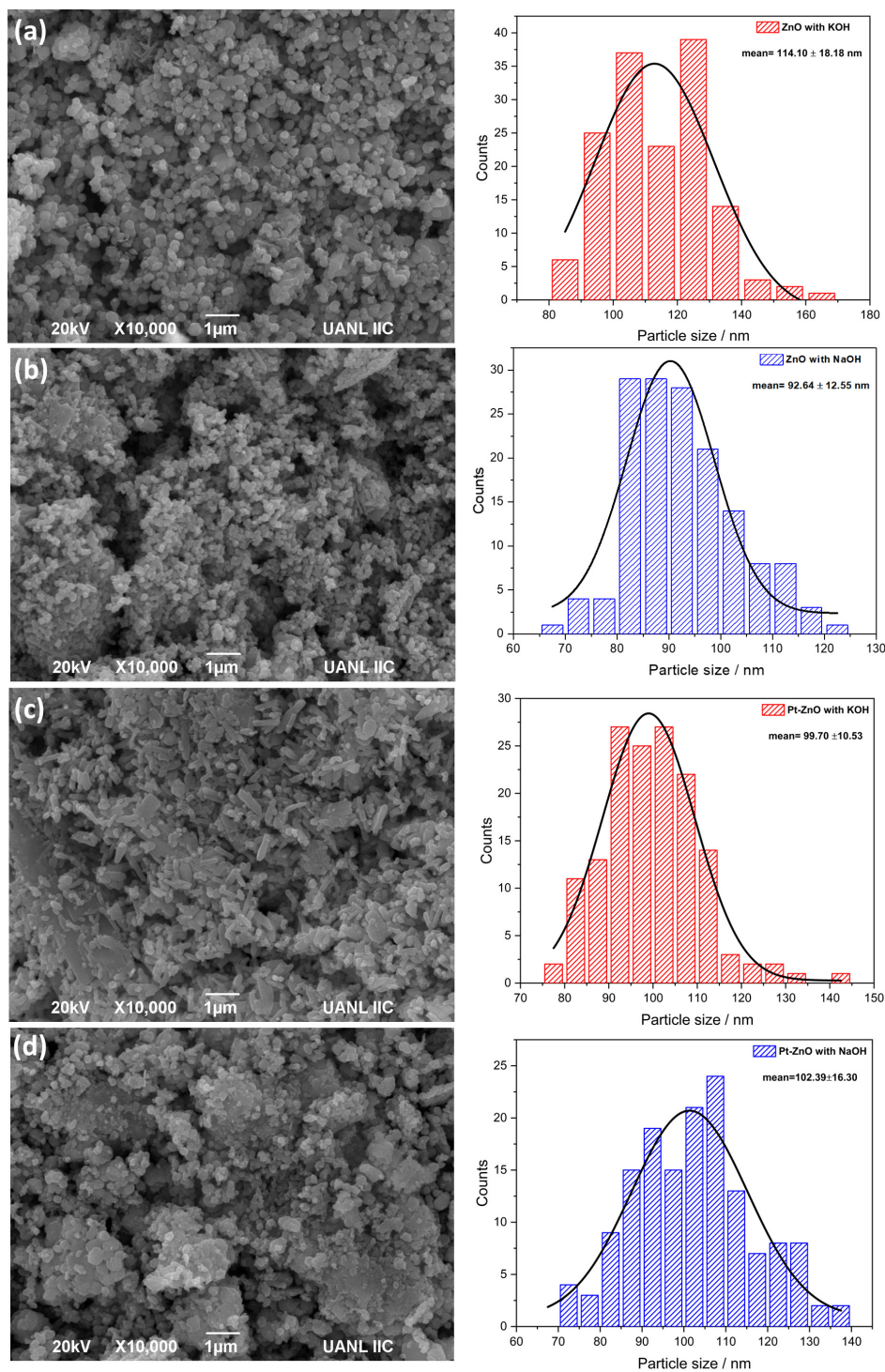The effect of precipitating agent NaOH on the size of

Figure 5. SEM images and particle size distribution of the ZnO obtained at KOH (a); NaOH (b) and Pt-ZnO obtained at KOH (c); NaOH (d).

particles is shown in Figures 5b and 5d. Adding NaOH makes particles smaller with the hexagonal and semi-spherical structure for ZnO and Pt-ZnO, respectively.

The structure change by adding Pt to ZnO can be seen in Figure 5c. Despite the initial structure of ZnO, a rod-like structure can be achieved. Such a structure is one of the best compared to others as they are one-dimensional structures that provide more efficient carrier transport due to decreased surface defects, disorder, and discontinuous interfaces,[44,45] as well as favor photocatalytic processes.[12]

According to the micrographs of Pt-ZnO NPs, smaller particle sizes are obtained with NaOH precipitating agent and larger particles with KOH precipitating agent. The opposite formation of Pt-ZnO impact oxide and the development of quantum properties on the surface causes these relocations in particle morphology. The increase in particle size can affect the photocatalytic processes by decreasing the rate constant.[23]

The growth of the nanocrystalline structure can be justified in terms of the polar surfaces of ZnO. The ZnO structure has alternating planes formed by coordinated tetrahedral O_2 and Zn^{2+} ions. Pt doping in the ZnO can cause certain planar defects, which can increase the surface energy and lead to accelerated anisotropic enhancement in different directions, which does not affect the intrinsic polarity of the nanostructures.[43]

The particle sizes obtained by SEM are larger than those obtained by X-ray due to the treatment of the samples at the time of each analysis and the agglomeration of the nanoparticles formed.[15]

Optical analysis by UV-Vis spectroscopy

Figure 6 shows the absorption spectra of ZnO and Pt-ZnO prepared with two different precipitating agents, KOH and NaOH. The absorption edge was found at 375 nm, confirming the activity in the UV-Vis region. The band gap was determined using the Tauc Plot method, graphing $(\alpha h\upsilon)^n$ *versus* $h\upsilon$. Four curves were plotted for the above values of "n" of 1/2, 2, 3/2, and 3 for direct allowed, indirect allowed, direct forbidden, and indirect forbidden, respectively. The best linear fit for the four synthesized nanomaterials (ZnO and Pt-ZnO) was obtained with the value of n = 2 for the $(\alpha h\upsilon)^2$-$h\upsilon$ curve. The largest band
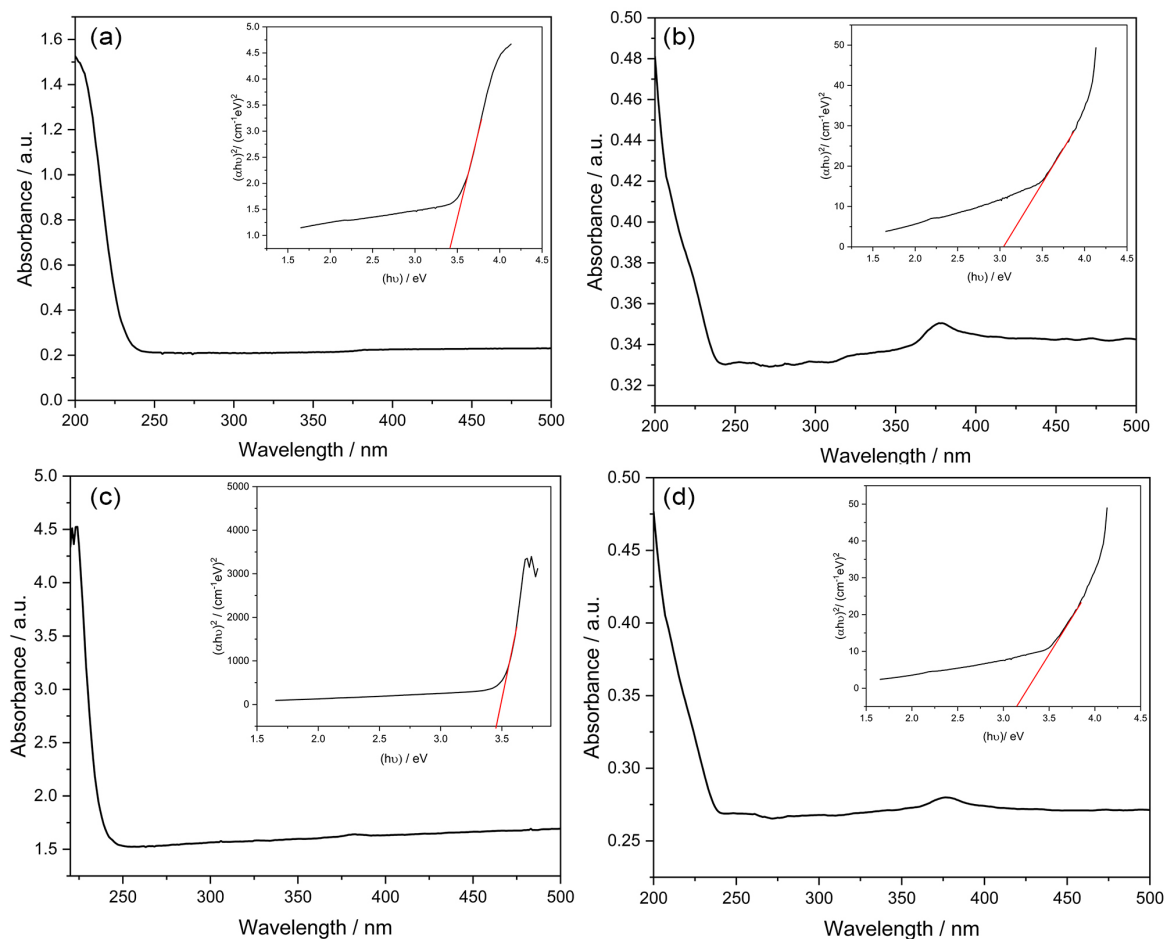

Figure 6. Band gap of the ZnO obtained at KOH (a), NaOH (b), and Pt-ZnO obtained at KOH (c), NaOH (d).

10 of 13

J. Braz. Chem. Soc. **2024**, *35*, 1, e-20230092

gap obtained from synthesizing the four nanocatalysts from the plot between hυ and $(\alpha h\upsilon)^2$ is 3.45 eV for Pt-ZnO with the precipitating agent KOH.

The results presented in this study coincide and exceed the values obtained with other investigations[45-52] (Table 3), supporting that Pt-ZnO NPs can be used as an efficacious catalyst for the degradation of recalcitrant compounds due to the high band gap of the synthesized nanomaterials, demonstrating the influence of the precursors used in the synthesis of the nanomaterials.

Table 3. The calculated average of structural parameters of the different synthesized materials

Material	Band gap / eV	
	Calculated	Literature
Al-ZnO	–	3.22[43]
ZnFe2O4	–	2.01[46]
ZnO/ZnFe$_2$O$_4$	–	1.88[46]
ZnO/ZnFe$_2$O$_4$/Pt-I	–	1.86[46]
ZnO/ZnFe$_2$O$_4$/Pt-II	–	1.67[46]
ZnO/ZnFe$_2$O$_4$/Pt-III	–	1.66[46]
ZnO	–	3.17[47]
ZnO	–	3.37[48]
ZnO	–	3.28[20]
V$_2$O$_5$-ZnO	–	2.64[20]
ZnO/Ag/Ag$_3$PO$_4$	–	3.13[49]
ZnO	–	3.24[50]
ZnO	–	3.21[51]
ZnO	–	3.16[52]
ZnO with KOH	3.39	–
ZnO with NaOH	3.05	–
Pt-ZnO with KOH	3.45	–
Pt-ZnO with NaOH	3.14	–

It is important to mention that obtained band gap obeys the interests of this research since the value is above the band gap of commercial ZnO, and one of the criteria to select a good photocatalyst is the high redox potential of the valence band, so that it is positive enough to make feasible the mineralization of contaminants. However, its photoactivation must be within the UV-Vis light range obtained for the four synthesized materials, demonstrating that the band gap increases as the crystal size increases in the materials.

As we have seen throughout this research, zinc oxide can be found in a wide variety of particle sizes, morphologies, and surface areas depending on the methodology and compounds used to perform the synthesis, the relationship between morphological, optical, and kinetic characteristics of photocatalytic reactions can be found in the literature.[52-54]

Conclusions

ZnO and Pt-ZnO semiconductors were obtained according to two different precipitating agents (KOH and NaOH) in an easy, and fast way by the modified direct precipitation method, which allowed corroborating and expanding the knowledge about the synthesis of these materials improving their functional characteristics concerning the results reported in the literature and to demonstrate the influence of using different precursors and precipitating agents in the synthesis of nanomaterials.

The results of the characterization of ZnO and Pt-ZnO by infrared spectroscopy show that the synthesis was carried out correctly since each one of the components that conform to each semiconductor are appreciated in their characteristic bands, being more pronounced the band of the ZnO synthesized with KOH. The scanning electron microscopy results show that the smallest crystal size was obtained with the precipitating agent NaOH, predominant semi-spherical conformations, and rod shapes; these morphological and structural characteristics would favor their use in photocatalytic processes as nanorods, nanowires, and nanotubes for the degradation of pollutants. XRD analyses showed hexagonal structure (wurtzite) formation for ZnO materials, obtaining a smaller crystal size in the nanoparticles synthesized with NaOH precipitating agent.

The success of the synthesis of the nanomaterials was demonstrated due to the high band gap obtained from Pt-ZnO synthesized with KOH precipitant, which exceeds the commercial band gap of ZnO, obtaining materials with excellent chemical, optical, electrochemical, and photocatalytic properties, which confirms that these nanomaterials effectively can be used as photocatalysts for the degradation of recalcitrant compounds.

Acknowledgments

References

1. Bekkari, R.; laânab, L.; Boyer, D.; Mahiou, R.; Jaber, B.; *Mater. Sci. Semicond. Process.* **2017**, *71*, 181. [Crossref]

2. Pérez Taborda, J. A.; Gallego, J. L.; Román, W. S.; Landázuri, H. R.; *Scientia Technica.* **2008**, *18*, 39. [Link] accessed in May 2023

3. Rosales-Gonzales, O.: *Síntesis y Caracterización de Catalizadores Pt/ZnO, Ni/ZnO y Pt-Ni/ZnO 1-D por el Método Hidrotermal para la Generación de H$_2$ por OSRM*; MSc Dissertation, Universidad Autónoma del Estado de Hidalgo, Hidalgo, Mexico, 2017. [Link] accessed in May 2023

4. Verdeja González, L. F.; García Coque, M. P.; Huerta Nosti, M. A.; *Rev. Minas* **1992**, *7*, 87. [Crossref]

5. Verdeja González, L. F.; García Coque, M. P.; Huerta Nosti, M. A.; *Bol. Soc. Esp. Ceram. Vidr.* **1993**, *32*, 267. [Link] accessed in May 2023

6. Tengfei, B.; Zhenxi, D.; Shuoyu, C.; Huan, H.; Xiaoming, S.; Yuechun, F.; *Appl. Surf. Sci.* **2023**, *614*, 156240. [Crossref]

7. Ghorbani, H. R.; Mehr, F. P.; *Orient. J. Chem.* **2015**, *31*, 1219. [Crossref]

8. Lucilha, A. C.; Afonso, R.; Silva, P. R. C.; Lepre, L. F.; Ando, R. A.; Dall'Antonia, L. H.; *J. Braz. Chem. Soc.* **2014**, *25*, 1091. [Crossref]

9. Amirulsyafiee, A.; Khan, M. M.; Harunsani, M. H.; *Catal. Commun.* **2022**, *172*, 106556. [Crossref]

10. Gines-Palestino, R.; Oropeza- De la Rosa, E.; Montalvo-Romero, C.; Cantú-Lozano, D.; *Rev. Mex. Ing. Quim.* **2019**, *19*, 639. [Crossref]

11. Jaramillo-Páez, C.; Navío, J.; Hidalgo, M.; Macías, M.; *Catal. Today* **2017**, *284*, 121. [Crossref]

12. Hasnidawani, J. N.; Azlina, H. N.; Norita, H.; Bonnie, N. N.; Ratim, S.; Ali, E. S.; *Procedia Chem.* **2016**, *19*, 211. [Crossref]

13. Olumurewa, K. O.; Eleruja, M. A.; *Phys. B* **2023**, *650*, 414588. [Crossref]

14. Xu, S.; Wang, Z. L.; *Nano Res.* **2011**, *4*, 1013. [Crossref]

15. Amador-Gómez, L. P.; Luna-Solano, G.; Urrea-García, G. R.; Gines-Palestino, R. S.; Cantú-Lozano, D.; *Processes* **2022**, *11*, 70. [Crossref]

16. Montalvo, C.; Gines, R. S.; Cantu, D.; Ruiz, A.; Aguilar, C.; Perez, I.; Ceron, R. M.; *Iran. J. Catal.* **2022**, *12*, 295. [Crossref]

17. Martinello Savi, B.; Rodríguez, L.; Michael Bernardin, A.; *QUALICER* **2012**. [Crossref]

18. Sanz Serrano, A.: *Nanopartículas de Óxido de Zinc para la Mejora de Dispositivos de Almacenamiento de Energía*; MSc Dissertation, Universidad Politécnica de Cartagena, Cartagena, España, 2016. [Link] accessed in May 2023

19. Shubha, J. P.; Roopashreeb, B.; Patil, R. C.; Mujeeb, K.; Shaik, M. R.; Alaqarbeh, M.; Alwarthan, A.; Karami, A. M.; Adil, S. F.; *Arabian J. Chem.* **2023**, *16*, 104547. [Crossref]

20. Shukla, P.; Shukla, J. K.; *J. Sci.: Adv. Mater. Devices* **2018**, *3*, 452. [Crossref]

21. Zhang, H.; Zhang, B.; Liang, F.; Fang, Y.; Wang, H.; Chen, A.; *Arabian J. Chem.* **2022**, *15*, 103951. [Crossref]

22. López-Cuenca, S.; Aguilar-Martínez, J.; Rabelero-Velasco, M.; Hernández-Ibarra, F. J.; López-Ureta, L. C.; Pedroza-Toscano, M. A.; *Rev. Mex. Ing. Quim.* **2019**, *18*, 1179. [Crossref]

23. Manikandana, B.; Muralib, K. R.; John, R.; *Iran. J. Catal.* **2021**, *11*, 1. [Crossref]

24. Friedmann, D.; *Appl. Catal. A* **2023**, *649*, 118943. [Crossref]

25. Aquino, P.; Osorio, A. M.; Ninána, E.; Torres, F.; *Rev. Soc. Quím. Perú* **2018**, *8*, 1.

26. Huang, J. S.; Lin, C. F.; *J. Appl. Phys.* **2008**, *103*, 014304.

27. González Vera, O. F.; Mutiz, J. J.; Urresta Aragón, J.; *Rev. Ion* **2017**, *30*, 31. [Crossref]

28. Putz, H.; *Match*, 3.0.0; Crystal impact, Bonn, Germany, 2015.

29. Rasband, W.; *ImageJ*, 2.0.0-rc-3; National Institutes of Health, USA, 2014.

30. Dianat, S.; *Iran. J. Catal.* **2018**, *8*, 121. [Crossref]

31. Debanath, M. K.; Karmakar, S.; *Mater. Lett.* **2013**, *111*, 116. [Crossref]

32. Pawar, V.; Pardeep, K.; Panda, S. K.; Priyanka, A.; Singh, P.; *Phys. Rev. Appl.* **2018**, *9*, 054001. [Crossref]

33. Kamarulzaman, N.; Kasim, M.; Rusdi, R.; *Nanoscale Res. Lett.* **2015**, *10*, 346. [Crossref]

34. Bindu, P.; Thomas, S.; *Acta Phys. Pol., A* **2017**, *131*, 1474. [Crossref]

35. Şimşek, T.; Ceylan, A.; Aşkin, G.; Özcan, S.; *J. Polytech.* **2022**, *25*, 89. [Crossref]

36. Medina, J. C.; Portillo-Vélez, N. S.; Bizarro, M.; Hernández-Gordillo, A.; Rodil, S. E.; *Dyes Pigm.* **2018**, *153*, 106. [Crossref]

37. Zafar, M.; Dar, Q.; Nawaz, F.; Zafar, M.; Iqbal, M.; Nazar, M.; *J. Mater. Res. Technol.* **2018**, *8*, 713. [Crossref]

38. Santos, L. K.; Cestari, A.; *Rev. Virtual Quim.* **2014**, *6*, 1021. [Crossref]

39. Cheng, N.; Lifen, L.; Rui, H.; *Sep. Purif. Technol.* **2018**, *206*, 316. [Crossref]

40. Pourrahimi, A. M.; Liu, D.; Pallon, L. K. H.; Andersson, R. L.; Abad, A. M.; Lagarón, J.-M.; Hedenqvist, M. S.; Ström, V.; Gedde, U. W.; Olsson, R. T.; *RSC Adv.* **2014**, *4*, 35568. [Crossref]

41. Hughes, W. L.; Wang, Z. L.; *Appl. Phys. Lett.* **2005**, *86*, 043106. [Crossref]

42. Wang, Z. L.; *ACS Nano* **2008**, *2*, 1987. [Crossref]

43. Mahdavi, R.; Talesh, S. S.; *Adv. Powder Technol.* **2017**, *28*, 1418. [Crossref]

44. Morkoç, H.; Özgür, Ü.; *Zinc Oxide Fundamentals, Materials, and Device Technology*; Wiley-VCH: Weinheim, 2009.

45. Moezzi, A.; McDonagh, A. M.; Cortie, M. B.; *J. Chem. Eng.* **2012**, *185-186*, 1. [Crossref]

46. Sobahi, T. R.; Amin, M. S.; *Ceram. Int.* **2020**, *46*, 3558. [Crossref]

47. Nimbalkar, A. R.; Patil, M. G.; *Phys. B* **2017**, *527*, 7. [Crossref]

48. Znaidi, L.; *Mater. Sci. Eng. B* **2010**, *174*, 18. [Crossref]

49. Du, C. Songa, J.; Tan, S.; Yanga, L.; Yu, G.; Chen, H.; Zhou, L.; Zhang, Z.; Zhanga, Y.; Su, Y.; Wen, X.; Wang, S.; *Mater. Chem. Phys.* **2021**, *260*, 124136. [Crossref]

50. Sánchez, C.; Doria, J.; Paucar, C.; Hernandez, M.; Mósquerra, A.; Rodríguez, J. E.; Gómez, A.; Baca, E.; Morán, O.; *Phys. B* **2010**, *405*, 3679. [Crossref]

51. Golsheikh, A. M.; Kamali, K. Z.; Huang, N. M.; Zak, A. K.; *Powder Technol.* **2018**, *329*, 282. [Crossref]

52. Lopes de Almeida, W.; Ferreira, N. S.; Severo Rodembusch, F.; Caldas de Sousa, V.; *Mater. Chem. Phys.* **2021**, *258*, 123926. [Crossref].

53. Silva Jr., R. S.; Matos, R. S.; Andrade, R.; Oliveira, R. M. P. B.; Resende, C. X.; Paz, S. P. A.; Angélica, R. S.; Ferreira, N. S.; *J. Mater. Res. Technol.* **2021**, *13*, 2006. [Crossref]

54. Lucca Sánchez, F. A.; Takimi, A. S.; Severo Rodembusch, F.; Pérez Bergmann, C.; *J. Alloys Compd.* **2013**, *572*, 68. [Crossref]